J. Earth Syst. Sci. (2020)129 78
https://doi.org/10.1007/s12040-020-1345-9

© Indian Academy of Sciences

Interpretation of resistivity data using 3D Euler deconvolution and Radially Averaged Power Spectrum

Shovana Mondal, Shalivahan Srivastava* and Ashok K Gupta

Department of Applied Geophysics, IIT (ISM), Dhanbad 826 004, India.
**Corresponding author. e-mail: shalivahan@iitism.ac.in*

MS received 6 July 2019; revised 9 November 2019; accepted 6 December 2019

Different electrode configuration in resistivity measurements over the same geologic structures generally produce different anomaly patterns. This is related to the position of the structure concerning the electrodes. Given the above, a unified approach has been proposed using the concept of analytical signal to interpret the resistivity data as electric potential follows Laplace's equation. We interpret the data sets using Euler deconvolution and Radially Averaged Power Spectrum (RAPS) to determine both lithological boundaries and units and compare the results with inverted resistivity section. We analysed the resistivity data using electrical resistivity tomography (ERT) technique over conducting dyke and vertical fault for Wenner and dipole–dipole arrays, respectively. The obtained structural indices for dyke and fault are 1.0 and 0.6, respectively. The results from Euler depth solutions match well with the inverted resistivity section. Subsequently, two field examples one each over ground water and mineral exploration were analysed. The delineated lineaments over ground water exploration matches fairly well with the available results. In addition, some additional lineaments are also mapped. These new features could be a zone of interest for a detailed survey. The depths from Euler depth solutions and RAPS are in agreement. However, no depth information was available earlier. The data for mineral exploration have been acquired by ERT technique with a profile length of ∼500 m over Dhanjori Basin, Jharkhand, India. The Euler depth solution and RAPS indicated the presence of two interfaces at an average depth of 8 and 20 m and 7 and 21 m, respectively. The first interface is present all along the profile, whereas the second interface lies between a part of the profile. The location and depth of these are in broad agreement with the resistivity sections obtained from ERT/AMT and borehole data. A borehole in the vicinity of the survey area indicated the presence of two interfaces. The first interface coincides with the soil depth and the second interface coincides with the sulphide mineralization.

Keywords. Resistivity; Euler deconvolution; Radially Averaged Power Spectrum (RAPS).

1. Introduction

Electrical resistivity survey is widely used in groundwater, mineral and geothermal reservoirs (Telford *et al.* 1990). Unlike, Vertical Electrical Sounding (VES) resistivity profiles present a bewildering variety of shapes (Chunduru *et al.* 1995) as it depends upon the array used (Bhattacharya and Srivastava 2016). Figure 1(a and b) shows the signal contribution sections for Wenner and dipole–dipole arrays (Barker 1979). The section shows the relative contributions made by individual volume elements of earth to the total potential difference measured between the potential electrodes. Figure 1(a) shows that the elements around each electrode makes large contributions to

Published online: 26 February 2020

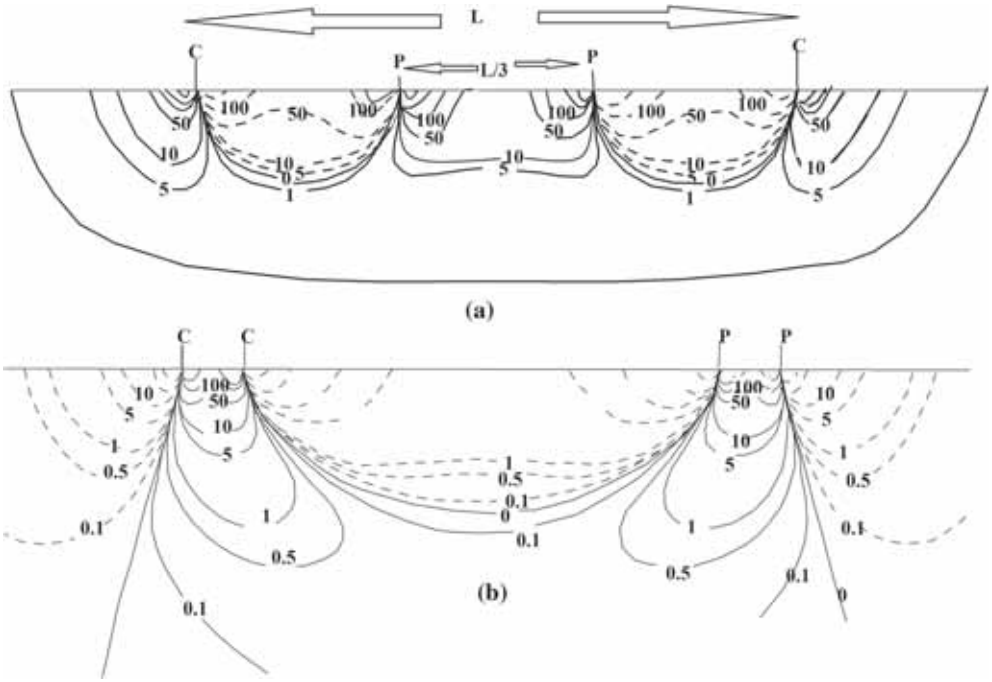

Figure 1. Signal contribution section for (**a**) Wenner array and (**b**) dipole–dipole array. Contours show the signal contribution; continuous and discontinuous lines shows for positive and negative contributions, respectively.

the total signal. In the close vicinity of each electrode, the contributions could be very large and would lead to singularity at the electrode at the ground surface. For a homogenous half-space the positive and negative contributions of high magnitude cancel each other and the resultant signal originates mainly from depth and not from the region around the electrodes. The flat nature of the signal contribution in the section (figure 1a) indicates that the vertical resolution is high as compared to lateral resolution in a Wenner configuration.

Figure 1(b) shows the signal contribution for dipole–dipole configuration. The signal originates from both positive and negative regions having larger vertical than horizontal extent indicating a large horizontal resolution as compared to vertical resolution.

The resistivity method uses a potential field and accordingly suffers from similar ambiguity problem to the gravity and magnetic methods. Since a potential field is involved, the apparent resistivity signature of any structure should be computed by a solution of Laplace's equation (Kearey *et al.* 2013). Eppelbaum (1999) analysed resistivity anomalies using tangent and characteristics point methods for interpreting magnetic data. Ekinci *et al.* (2014) acquired geomagnetic and geoelectrical data sets over buried archaeological remains. They obtained the Euler depth solutions of the geomagnetic data and compared the results with the inversion of resistivity data sets. The obtained Euler depth solutions were in agreement with the inverted sections.

As the electrical potential satisfies Laplace's equation, an attempt has been made to interpret resistivity data obtained from Electrical Resistivity Tomography (ERT) technique and Wenner array using Euler homogeneity equation (Thompson 1982) and radially averaged power spectrum (Spector and Grant 1970) both for synthetic and field examples.

2. Methodology

For the sake of completeness and clarity, we briefly describe the Euler deconvolution and Radially Averaged Power Spectrum (RAPS) interpretational tools.

2.1 *Analytical signal*

Nabhighian (1972) introduced the concept of analytical signal of magnetic anomaly over the horizontal faulted slabs. The amplitude of analytical signal is the square root of the sum of the

squares of the first-order horizontal and vertical derivatives. These derivatives are related by Hilbert transform pair.

Potential field function satisfying Laplace's equation in 2D is represented by $V(x)$. $|A(x)|$, analytical signal can be written as

$$A(x) = \frac{\partial V}{\partial x} - i\frac{\partial V}{\partial z}. \tag{1}$$

And the amplitude of 2D analytical signal is given by

$$|A(x)| = \sqrt{\left(\frac{\partial V}{\partial x}\right)^2 + \left(\frac{\partial V}{\partial z}\right)^2}, \tag{2}$$

where, $\left(\frac{\partial V}{\partial x}\right)$ and $\left(\frac{\partial V}{\partial z}\right)$ are the first-order horizontal and vertical derivatives of potential, respectively.

2.2 *3D Euler deconvolution*

Thompson (1982) obtained the depth and horizontal location of the causative source for the magnetic anomaly using Euler deconvolution by assuming the source geometry. An approach of Euler deconvolution based on the equation of Euler homogeneity was given by Blakely (1995) to locate the causative source and to estimate the depth for potential field data. Mathematically, it can be expressed as:

$$(x - x_0)\frac{\partial V}{\partial x} + (y - y_0)\frac{\partial V}{\partial y} + (z - z_0)\frac{\partial V}{\partial z} = -nV. \tag{3}$$

Here, the location of the anomalous source at (x_0, y_0, z_0), the total field V is the potential and n is the structural index that relates to the geometry of the source. This technique uses first-order horizontal and vertical derivatives. The first-order derivatives are used as a high frequency enhancement filters (Agarwal and Lal 1972a, b). If noise is present in the high frequency data then it gets enhanced and eventually the response of the target is masked. Further, the utility of these first-order derivatives depends upon the depth of the burial of anomalous sources (Agarwal and Srivastava 2009).

Total field gradient is calculated from 3D Euler deconvolution to obtain solutions within a small convolution window using Oasis Montaj (Geosoft 2007). The window size is adjusted throughout the grid to determine the horizontal and vertical location of the source to a given structural index (Yadav *et al.* 2018). A solution of the least square method yields the uncertain location of the source. However, reliable solutions can be obtained by selecting proper window size, structural index and depth tolerance. The suitable structural index is chosen by the earlier geological knowledge. The applicability of this method on real data sets reveal the high potentiality of technique in interpreting anomalies over complex source geometries and can be applied on a routine basis.

2.3 *Radially Averaged Power Spectrum (RAPS)*

Radially averaged means the powers for equal lengths of the wave-vectors are averaged. Power spectrum $p(\omega)$ is the square of the Fourier amplitude spectrum (Spector and Grant 1970). Fast Fourier Transform (FFT) is applied to calculate the energy spectrum. Depth can be estimated from the slope of the energy spectrum curve (Spector and Grant 1970). The mathematical expression of power spectrum $p(\omega)$ is related to depth (h) as:

$$p(\omega) \sim e^{-2\omega h}. \tag{4}$$

In the above equation, ω is the wavenumber and h is the depth of the source (Yadav *et al.* 2018). Depth to source can be derived directly from the slope of the log radially averaged power spectrum. The depth determined from power spectrum–wavenumber plot is expressed as:

$$h = -\frac{s}{4\pi}, \tag{5}$$

where, s is the slope of the log energy spectrum.

The slope of smaller and higher wavenumber region indicates deeper depth and the shallower depth, respectively. These method calculate the average depth of the different segments according to the slope.

3. Results

To appraise the effect of the proposed Euler deconvolution technique, we have simulated two synthetic models, namely, dyke, fault and two field examples. The apparent resistivity data for the synthetic models have been obtained from RES2DMOD software (Loke and Barker 1996). The field examples have been adapted from published literature.

3.1 *Analyses of synthetic data*

3.1.1 *Dyke*

Figure 2(a) shows the model of conducting dyke of width 20 m at a depth of 15 m. The assumed dyke has a resistivity of 10 Ωm embedded in a host rock of 1000 Ωm. The thickness and resistivity of the overburden is 15 m and 300 Ωm, respectively. The pseudo-section for sixteen different depth levels using Wenner array was generated for a profile length of 300 m at an electrode spacing of 5 m. The assumed dyke is at the centre of the profile. Figure 2(b) shows the Euler depth solution of dyke with structural index (SI) of 1 superimposed over the inverted resistivity section. The index of figure 2(b) shows that the maximum number of solution (58.3%) lies between ∼−6.0 and −17.0 m with an average depth of −13.67 m. The second tightest cluster (35.2%) is for the depth range of ∼−17.0 to −28.0 m with an average depth of ∼21.5 m. The obtained Euler solutions are in broad agreement with the inverted model with respect to the depth.

The vertical boundary of the dyke has been obtained using the power spectrum (RAPS) (Spector and Grant 1970). Figure 3 shows the RAPS map of conducting dyke resistivity data. It is observed that the map of the dyke shows depth boundary at depth ∼16.64 m.

3.1.2 *Vertical fault*

Figure 4(a) shows the geometry of the considered vertical fault. The pseudo-section at 10 different depth levels was generated using a dipole–dipole arrangement for a profile length of 50 m with electrode spacing of 1 m. The fault is assumed at a depth of 0.75 m and the fault plane is at 28 m. The tightest cluster of the Euler depth solutions (figure 4b) have been obtained for window size and SI 8 and 0.6, respectively. The index of figure 4(b) shows that the maximum number of solution (62.7%) lies between the depth range of ∼−0.05 to −1.4 m with an average depth of −0.5 m. The second tightest cluster (30.6%) is for the depth range of ∼−1.4 to −2.8 m with an average depth of ∼1.85 m. The obtained Euler solutions are in broad agreement with the inverted model with respect to edges and the depth. The Euler depth solution when superimposed over inverted model (figure 4b) shows that the Euler depth solutions are in agreement with the model. Figure 5 shows the RAPS map of the apparent resistivity data for the considered vertical fault. It is observed that the map show depth boundary at depth −1.05 m.

3.2 *Field examples*

3.2.1 *Bakonyjako Horst, Hungary*

Figure 6(a) is the conductance map over Bakonyjako Horst, Hungary bauxite deposits adapted from Palacky *et al.* (1981). The data were acquired using a central gradient electrical resistivity survey. The Bakonyjako Horst is bounded by sub-vertical faults. On the down thrust sides, the thickness of the sediments exceeds 300 m and some bauxite deposits are found in this area.

The tightest cluster of Euler depth solutions was obtained with window size and SI of 12 and 0.6,

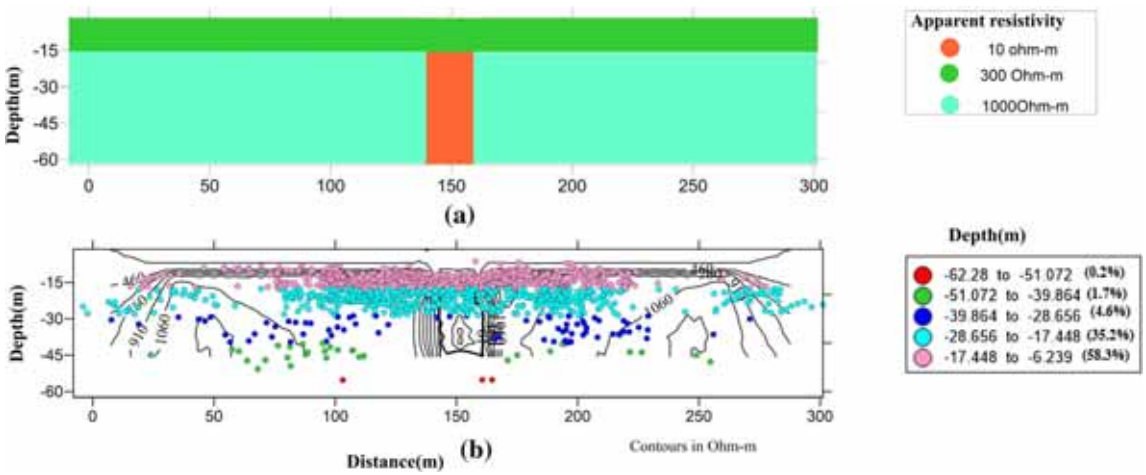

Figure 2. (**a**) Dyke model and (**b**) Euler depth solution of dyke with SI 1 for Wenner array superimposed over the inverted model resistivity section. This shows the depth range along with % of solutions in the specified range.

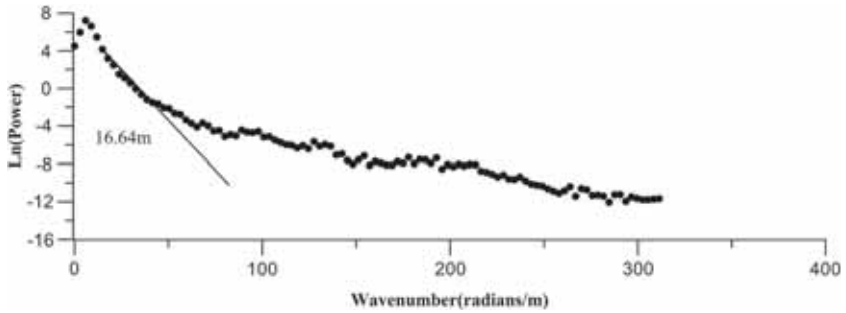

Figure 3. Radially averaged power spectrum of resistivity data for model figure 2(a).

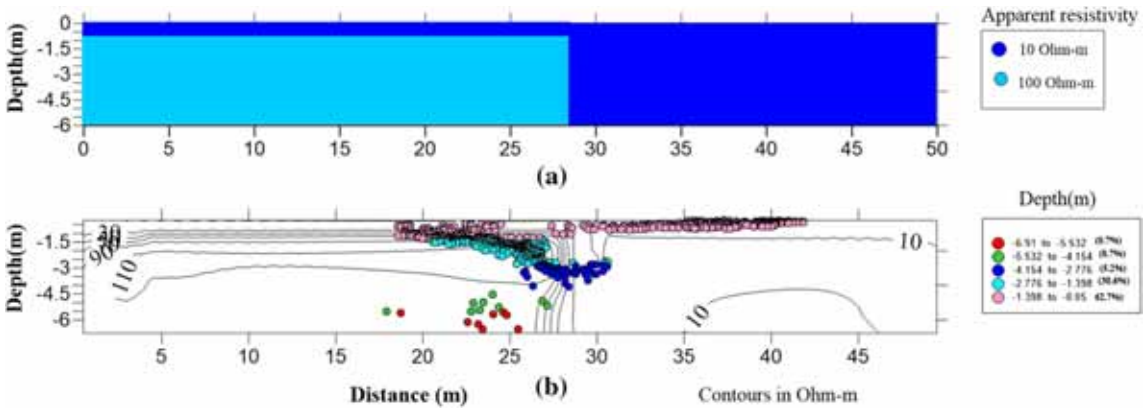

Figure 4. (**a**) Vertical fault model and (**b**) Euler depth solution of vertical fault with SI 0.6 for dipole–dipole array. The index shows the depth range along with % of solutions in the specified range.

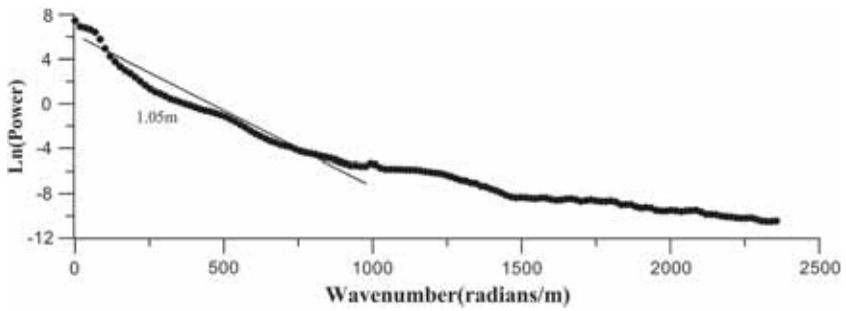

Figure 5. Radially averaged power spectrum of resistivity data for model figure 4(a).

respectively. The black filled circles (figure 6a) shows the fault zone as indicated by Kilenyi and Szabo (1985). However, they could not obtain the depth of these lineaments. The Euler depth solutions delineate both these lineaments reasonably well. Apart from these two lineaments, couple of more lineaments have been delineated (figure 6a) which was not available in the map of Kilenyi and Szabo (1985). Figure 6(b) shows the depth distribution of clustered Euler solution. The maximum number of solution (48.87%) lies between ∼−45.0 and −81.0 m with an average depth of ∼−62.5 m. The second tightest cluster (38.4%) is for the depth range of ∼−10.0 to −45.0 m with an average depth of ∼34.0 m. The third tightest cluster 14% is in the depth range of about ∼81–116 m with an average depth of about 93 m. The thicknesses delineated from RAPS maps show that the three mapped interfaces are at ∼21, 66, and 143 m, respectively (figure 7).

3.2.2 *Dhanjori metavolcanics, eastern India*

The study area is near Dublabera, bounded within the Dhanjori Basin in the East-Singhbhum,

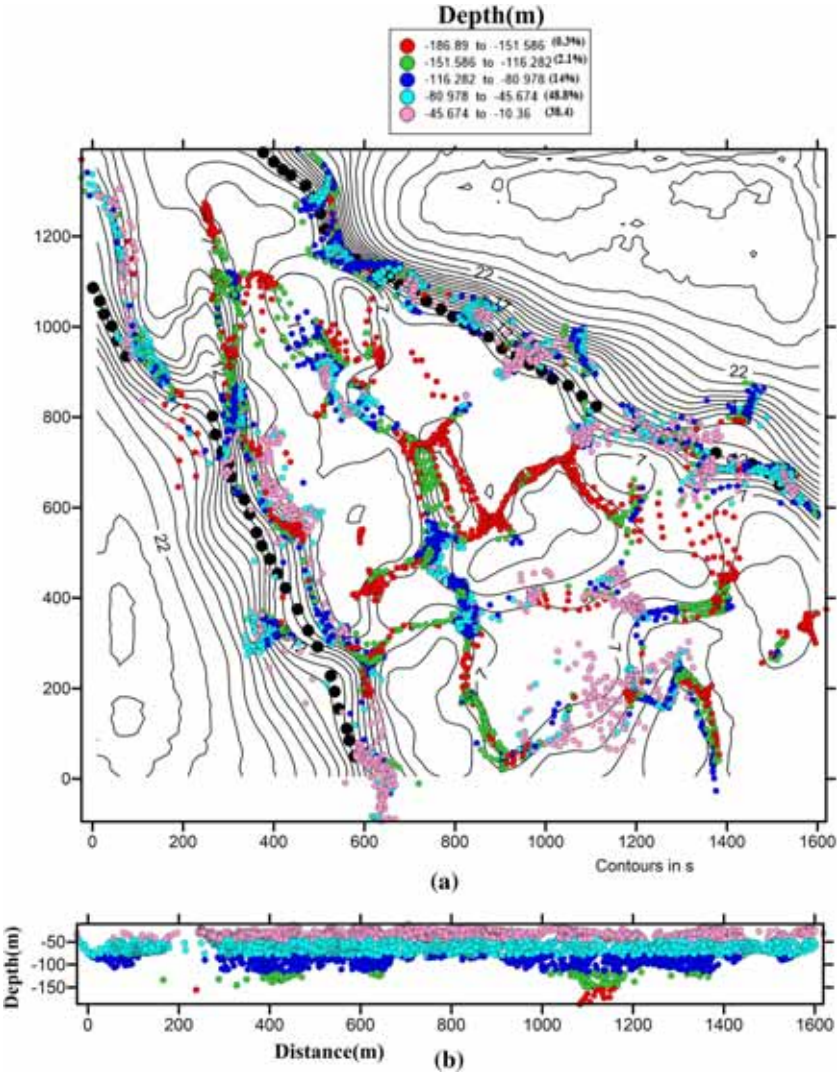

Figure 6. (**a**) Euler solution of conductance map of sub-vertical fault. The tightest cluster was obtained for SI 0.6. The black filled circles show the fault mapped by Kilenyi and Szabo (1985). The contour shows conductance. (**b**) Depth distribution of cluster Euler solution on x–z plane. The index shows the depth range along with % of solutions in the specified range.

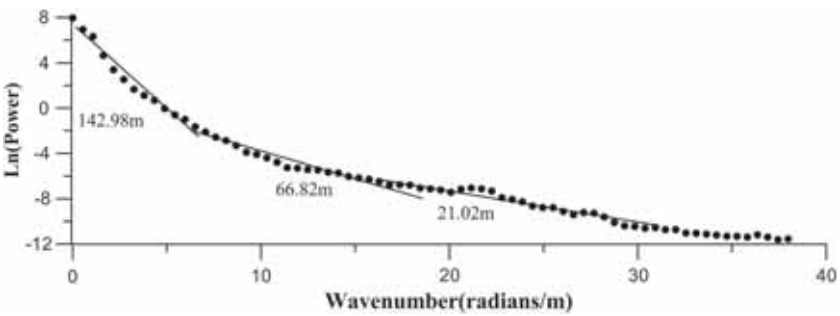

Figure 7. Radially averaged power spectrum of conductance of figure 6.

Jharkhand, India. The Dhanjori group of rocks consist of meta-sedimentary units, volcanic and volcanogenic sediments of Proterozoic greenstone assemblage (Gupta *et al.* 1985, and others). The major constituents of the Dhanjori group are lower Dhanjori and upper Dhanjori volcanic. The mineralization is associated with lower Dhanjori (Gupta *et al.* 1985; Mazumder and Sarkar 2004). Gupta *et al.* (2019) acquired resistivity data using a dipole–dipole array with the help of ERT technique

with a dipole separation of 10 m. The data have been acquired along eight west-east parallel lines with a profile length of ∼500 m and separation of 50 m between two consecutive lines. The data were acquired for dipole separation factor (n) up to eight for each line. Singh *et al.* (2019) analysed audio magnetotelluric (AMT) data sets over the same region.

We interpreted the data for all values of dipole separation using Euler depth solution and RAPS. Figure 8(a–f) shows the Euler solutions and RAPS for two representative dipole separation factor $n = 1$ and 3. The tightest Euler solutions were obtained for SI = 1.0. It can be seen from figures 8(a) (top) and 8(d) (top) that the causative source (A and B) extends for both the dipole separation factor for all the lines.

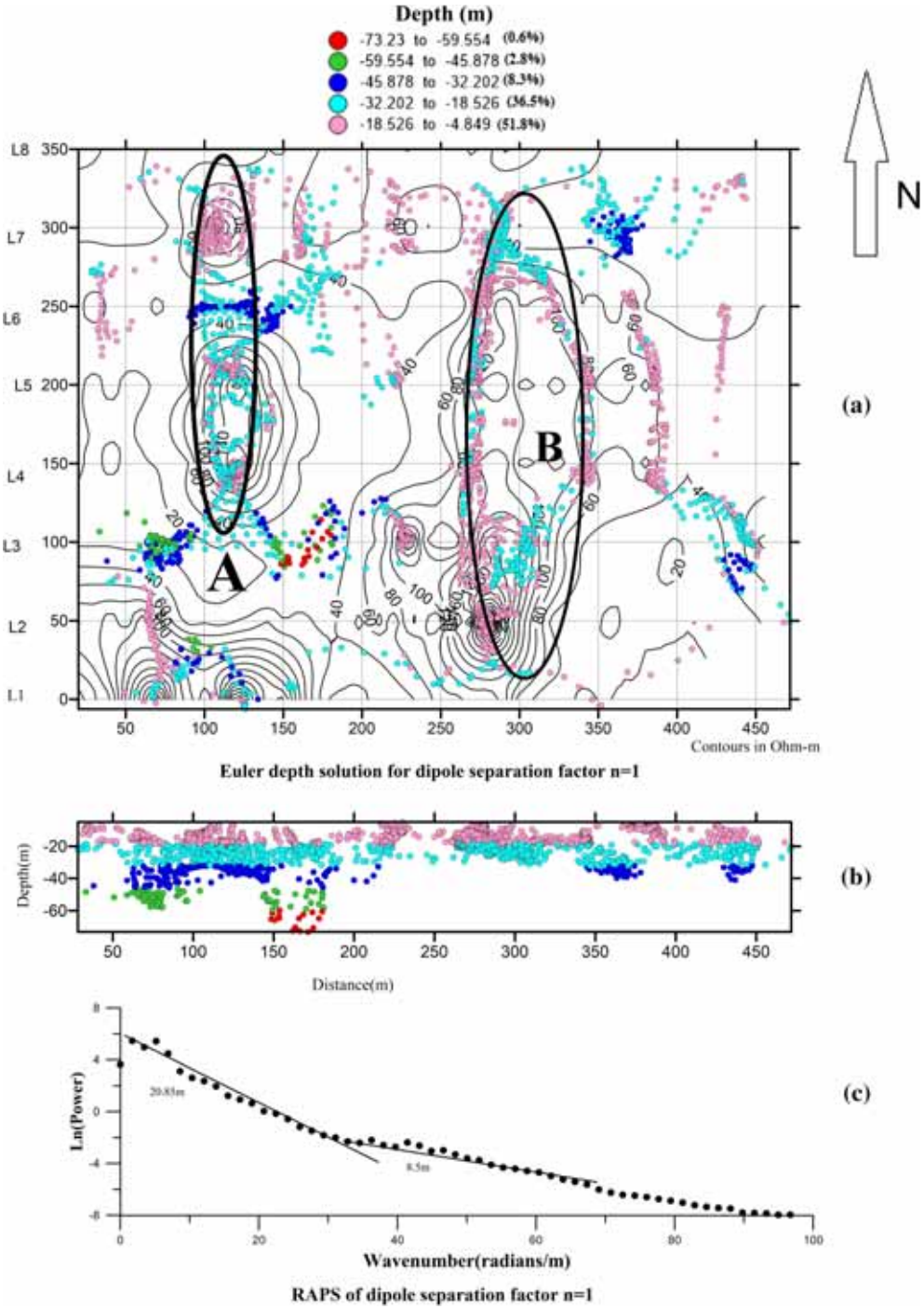

Figure 8. Euler depth solutions (top), depth distribution of clustered Euler solutions (middle) and RAPS (bottom) for dipole separation factor (**a–c**) $n = 1$, (**d–f**) $n = 3$. The index shows the depth range along with % of solutions in the specified range. L1 , . . . , L8 are the eight ERT lines along which the data have been acquired.

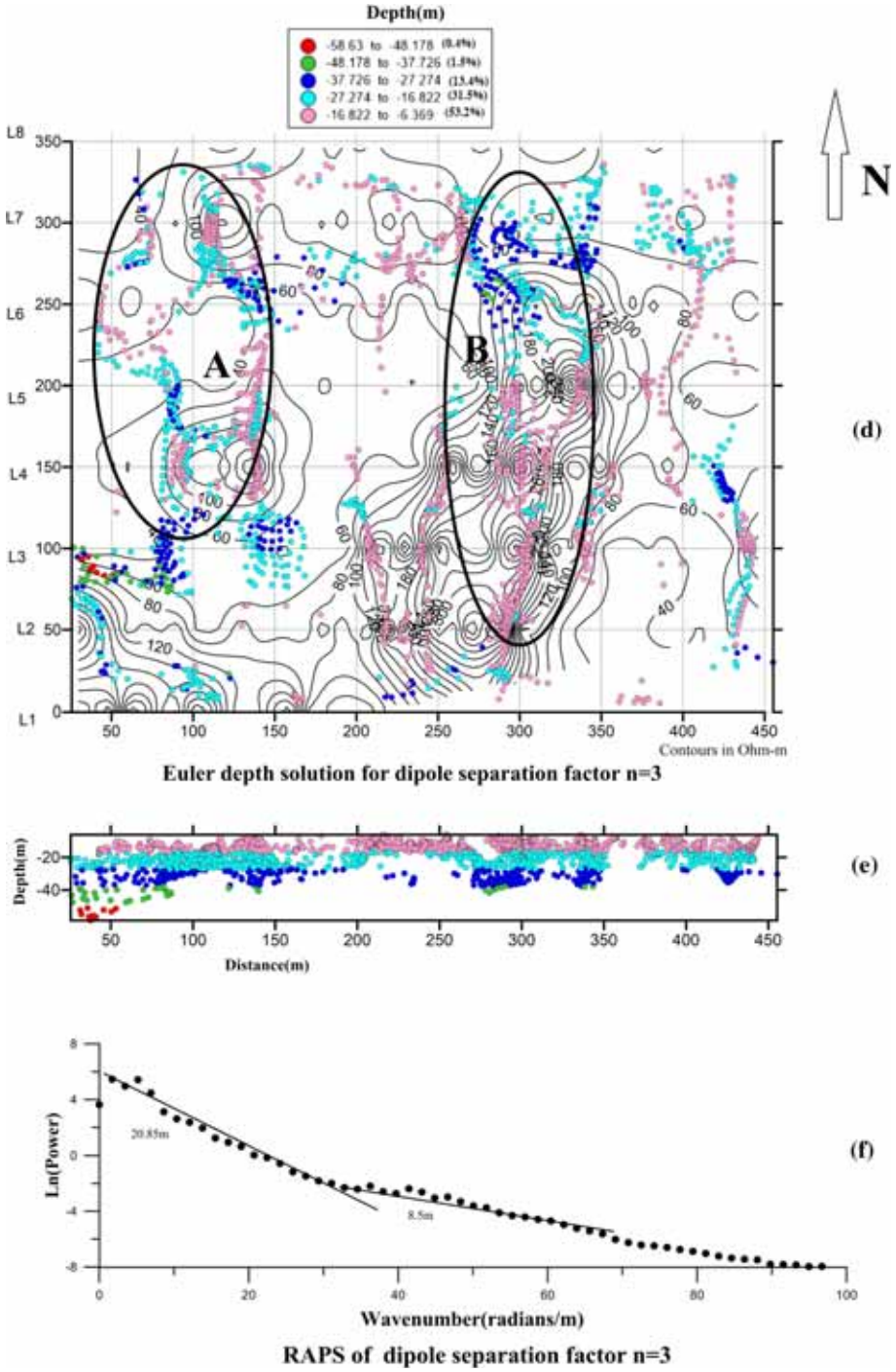

Figure 8. (*Continued.*)

Figures 8(b) (middle) and 8(e) (middle) shows the depth distribution of clustered Euler solutions. RAPS analysis (figures 8c (bottom) and 8f (bottom)) shows that the depths are ∼33, 21, and 10 m. It shows that the Gupta *et al.* (2019) inverted the data sets and obtained weathered layer, Quartz vein/QPC with disseminated sulphide ± auriferous concentrations, Greenstone schist/phyllite, Metabasalt/proterozoic gabbroic anorthosite ultramafic (PGAU) intrusion/ younger dolerite and massive sulphides. We performed Euler depth solutions and RAPS on the representative Line 4. The inverted resistivity model section as obtained by Gupta *et al.* (2019) is shown in figure 9. The tightest cluster of Euler depth solutions was obtained with window size and SI of 10 and 1, respectively. The Euler solutions are superimposed on inverted resistivity model section, figure 9. All along an interface with an average depth of ∼8 m is

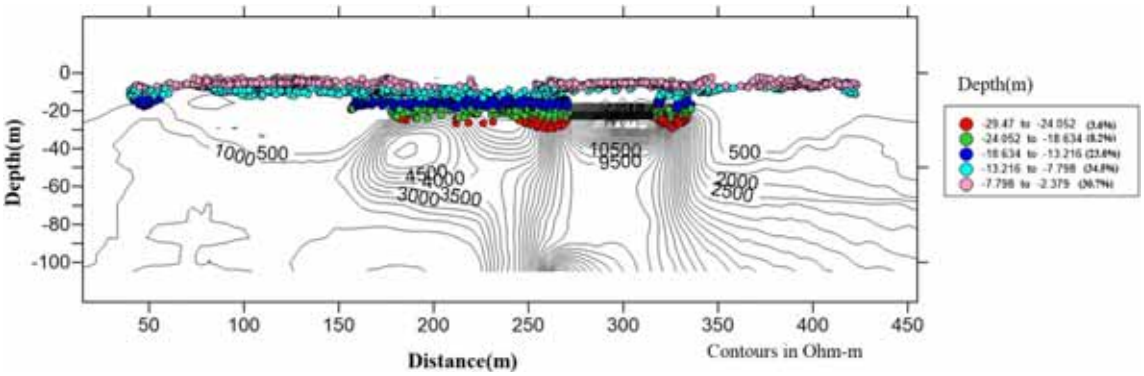

Figure 9. Euler depth solution of apparent resistivity superimposed on inverted model resistivity section for Line 4. The index shows the depth range along with % of solutions in the specified range.

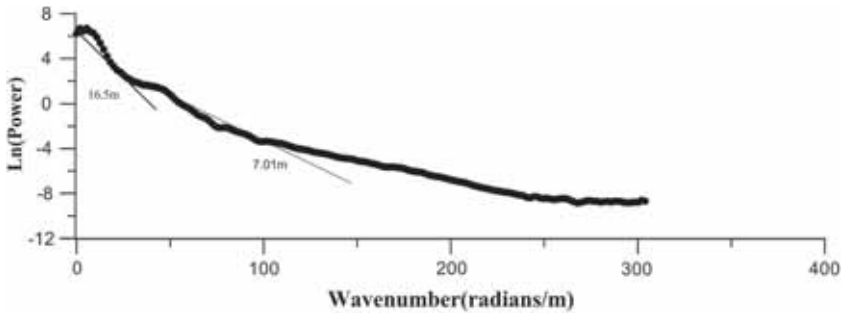

Figure 10. Radially averaged power spectrum of apparent resistivity data for Line 4 for Dhanjori data.

obtained which coincides with weathered layer. The resistor in between 290 and 350 m coincides with Quartz vein/QPC with disseminated sulphide ± auriferous concentrations (Gupta *et al.* 2019). At the edges of this mineralization, the average depth of the clustered solution is ∼18 m. Gupta *et al.* (2019) obtained depths of ∼10 and 20 m for weathered layer and QPC mineralization for Line 4. The solutions are in broad agreement with the inverted resistivity model section.

RAPS analysis (figure 10) of the Line 4 indicated two interfaces ∼7 and 15 m, respectively. Singh *et al.* (2019) inverted the AMT data along Line 4 and obtained interfaces at 10 and 20 m. A Borehole at a distance of ∼10 km in the eastern part of the study area was drilled up to 350 m (Das *et al.* 2008). The borehole up to 50 indicated soil depth up to 7 m underlain by meta basalts with grains of pyrite varying from 0.5% to 1.5%. The obtained depth solutions from Euler deconvolution and RAPS are in broad agreement with those obtained by Gupta *et al.* (2019) and Singh *et al.* (2019) and borehole data. The two interfaces from the present study may be interpreted as soil depth (first layer) and sulphide mineralization (second layer).

4. Conclusion

A unified approach for interpreting the resistivity anomalies of the different arrays have been discussed using Euler deconvolution and Radially Averaged Power Spectrum (RAPS) to determine lithological boundaries and lithological units. Euler deconvolution determines the location, the depth and the geometry of the causative source. At first two synthetic models for vertical conducting dyke and the vertical fault has been considered. The data have been generated using ERT techniques for Wenner and dipole–dipole arrays for dyke and fault, respectively. The tightest cluster for Euler depth solutions were obtained for structural index 1 and 0.6 for dyke and fault, respectively. The obtained depths match well with the assumed depths. Euler depth solutions matches well and follow the inverted model resistivity section.

Two field examples adapted from published literature have been analysed. In one of the field example, the faults were delineated. Earlier published results indicated only two lineaments without any idea about the depth. The obtained Euler solutions mapped these features reasonably well. In

addition, some more lineaments have been identified. The present study identifies linear trends and also determines the depth of these features. The delineated faults match well with the earlier results. Euler depth solutions and RAPS over Dhanjori meta-volcanics shows interfaces at 10 and 20 m and 10 and 5 m, respectively. The obtained results match fairly well with the available inverted resistivity structures from ERT/ AMT studies and the available borehole in the vicinity of the study area. The second interface is interpreted as sulphide mineralization. The ERT data for different dipole separation can help in identifying trends corresponding to these separation. 3D inversion is required for interpretation of grid data. However, Euler solutions for different dipole separation factor can help in identifying trends and depths which can help in field planning and constrained inversion.

References

Agarwal B N P and Lal T 1972a Calculation of the vertical gradient of the gravity field using the Fourier transform; *Geophys. Prospect.* **20** 448–458.

Agarwal B N P and Lal T 1972b A generalized method of computing second derivative of gravity field; *Geophys. Prospect.* **20** 385–394.

Agarwal B N P and Srivastava S 2009 Analyses of self-potential anomalies by conventional and extended Euler deconvolution techniques; *Comput. Geosci.* **35(11)** 2231–2238.

Barker R D 1979 Signal contribution sections and their use in resistivity studies; *Geophys. J. Int.* **59** 123–129.

Bhattacharya B B and Srivastava S 2016 Geoelectric methods: Theory and applications, McGraw Hill Education, India.

Blakely R J 1995 Potential theory in gravity and magnetic applications, Cambridge University, Cambridge.

Chunduru R K, Sen M K, Stoffa P L and Nagendra R 1995 Non-linear inversion of resistivity profiling data for some regular geometrical bodies; *Geophys. Prospect.* **43** 979–1003.

Das L K, Dasgupta K K and De M K 2008 Mineral potential of Dhanjori Metavolcanics, East Singhbhum, Jharkhand; *Indian Miner.* **61** 193–200.

Ekinci Y L, Balkaya, Ç, Şeren A, Kaya M A and Lightfoot C S 2014 Geomagnetic and geoelectrical prospection for buried archaeological remains on the Upper City of Amorium, a Byzantine city in midwestern Turkey; *J. Geophys. Eng.* **11(1)** 015012.

Eppelbaum L V 1999 Quantitative interpretation of resistivity anomalies using advanced methods developed in magnetic prospecting; *Trans. XXIV Gen. Assem. Eur. Geophys. Soc. Strasbg.* **1(1)** 166.

Geosoft Program (Oasis Montaj) 2007 Geosoft Mapping and Application System Inc. Suit 500, Richmond St. West Toronto, ON Canada N5SIV6.

Gupta A, Basu A and Singh S K 1985 Stratigraphy and petrochemistry of Dhanjori greenstone belt, eastern India; *Q. J. Geol. Min. Metall. Soc. India*, 248–263.

Gupta A K, Singh R K and Shalivahan 2019 Investigation of auriferous mineralization over Greenstone Schist Belt of Dhanjori Basin, Eastern India using 2-D Electrical Resistivity Tomography and Induced Polarization surveys; *Explor. Geophys.* **50** 364–375.

Kearey P, Brooks M and Hill I 2013 An introduction to geophysical exploration, John Wiley & Sons, Hoboken.

Kilenyi E and Szabo Z 1985 History and present state of the art of geophysics in Hungary; *First Break* **3** 9–23.

Loke M H and Barker R D 1996 Rapid least-squares inversion of apparent resistivity pseudo-sections by a quasi-Newton method 1; *Geophys. Prospect.* **44(1)** 131–152.

Mazumder R and Sarkar S 2004 Sedimentation history of the Palaeo proterozoic Dhanjori Formation, Singhbhum, Eastern India; *Precamb. Res.* **130** 267–287.

Nabhighian M N 1972 The analytical signal of 2D magnetic bodies with polygonal cross-section: Its properties and use for automated anomaly interpretation; *Geophysics* **37** 507–517.

Palacky G J, Ritsema I L and Jong S D 1981 Electromagnetic prospecting for groundwater in Precambrian terrains in the Republic of Upper Volta; *Geophys. Prospect.* **29** 932–955.

Spector A and Grant F S 1970 Statistical models for interpreting aeromagnetic data; *Geophysics* **35** 293–302.

Singh R K, Maurya V P and Singh S 2019 Imaging Regional Geology and Au–Sulphide mineralization over Dhanjori greenstone belt: Implications from 3-D Inversion of Audio Magnetotelluric data and Petrophysical Characterization; *Ore Geol. Rev.* **106** 369–386.

Thompson D T 1982 EULDPH – A new technique for making computer assisted depth estimates from magnetic data; *Geophysics* **47** 31–37.

Telford W M, Geldart L P and Sheriff R E 1990 *Applied Geophysics*, Cambridge University, Cambridge.

Yadav P K, Adhikari P K, Srivastava S, Maurya V P, Tripathi A, Singh S, Singh R K and Bage A K 2018 Lithologic boundaries from gravity and magnetic anomalies over Proterozoic Dalma volcanics; *J. Earth Syst. Sci.* **127(2)**, https://doi.org/10.1007/s12040-018-0918-3.

Corresponding editor: Arkoprovo Biswas